Human Molecular Genetics, 2009, Vol. 18, No. 23 ***4552–4564***
doi:10.1093/hmg/ddp421
Advance Access published on September 24, 2009

Mutant SOD1 in neuronal mitochondria causes toxicity and mitochondrial dynamics abnormalities

Jordi Magrané[§], Isabel Hervias[§,†], Matthew S. Henning, Maria Damiano[‡], Hibiki Kawamata and Giovanni Manfredi*

Department of Neurology and Neuroscience, Weill Medical College of Cornell University, New York, NY 10065, USA

Received May 29, 2009; Revised and Accepted August 28, 2009

Amyotrophic lateral sclerosis (ALS) is a fatal neurological disorder characterized by motor neuron degeneration. Mutations in Cu,Zn-superoxide dismutase (SOD1) are responsible for 20% of familial ALS cases via a toxic gain of function. In mutant SOD1 transgenic mice, mitochondria of spinal motor neurons develop abnormal morphology, bioenergetic defects and degeneration, which are presumably implicated in disease pathogenesis. SOD1 is mostly a cytosolic protein, but a substantial portion is associated with organelles, including mitochondria, where it localizes predominantly in the intermembrane space (IMS). However, whether mitochondrial mutant SOD1 contributes to disease pathogenesis remains to be elucidated. We have generated NSC34 motor neuronal cell lines expressing wild-type or mutant SOD1 containing a cleavable IMS targeting signal to directly investigate the pathogenic role of mutant SOD1 in mitochondria. We show that mitochondrially-targeted SOD1 localizes to the IMS, where it is enzymatically active. We prove that mutant IMS-targeted SOD1 causes neuronal toxicity under metabolic and oxidative stress conditions. Furthermore, we demonstrate for the first time neurite mitochondrial fragmentation and impaired mitochondrial dynamics in motor neurons expressing IMS mutant SOD1. These defects are associated with impaired maintenance of neuritic processes. Our findings demonstrate that mutant SOD1 localized in the IMS is sufficient to determine mitochondrial abnormalities and neuronal toxicity, and contributes to ALS pathogenesis.

INTRODUCTION

Amyotrophic lateral sclerosis (ALS) is a devastating neurodegenerative disease resulting in a rapidly progressive paralysis due to degeneration of motor neurons. Sporadic ALS represents 90% of the cases, whereas familial ALS accounts for the remaining 10%. Among the familial forms, 20% are caused by mutations in the gene encoding Cu,Zn-superoxide dismutase (SOD1).

The mechanism underlying the selective degeneration and death of motor neurons in SOD1 familial ALS are still largely unknown, but it is clear that mutant SOD1 exerts a toxic gain of function. There are several hypotheses for mutant SOD1 toxicity, which are non-mutually exclusive (1), including the contribution of mitochondrial dysfunction (2) and axonal transport abnormalities (3). Mice expressing G93A mutant human SOD1 (hSOD1) develop mitochondrial bioenergetic impairment in the spinal cord (4–6). In brain and spinal cord of mutant SOD1 transgenic mice, there is decreased mitochondrial Ca^{2+} capacity early on in the course of the disease (7). Mitochondrial dysfunction has also been observed in cultured cells expressing mutant SOD1 (8). Furthermore, mitochondrial morphological abnormalities are early signs of mutant SOD1 toxicity, and appear both in the cell bodies (9) and in the terminal axons of motor neurons (10). Accumulation of abnormal mitochondria may be caused by a block of axonal transport into proximal neurites (11) or impairment of mitochondria recycling and dynamics (12).

A substantial amount of SOD1 is found in mitochondria (5,13–21), predominantly in the spinal cord (22). Accumulation of mutant SOD1 is associated with mitochondrial

*To whom correspondence should be addressed at: Department of Neurology and Neuroscience, Weill Medical College of Cornell University, 525 E. 68th Street, A-505, New York, NY 10065, USA. Tel: +1 2127464605; Fax: +1 2127468276; Email: gim2004@med.cornell.edu
§The authors wish it to be known that, in their opinion, the first two authors should be regarded as joint First Authors.
†Present address: Department of Pharmacology, University of Navarra, Pamplona, Spain.
‡Present address: URA CEA-CNRS 2210, Service MIRCen, Institut d'Imagerie Biomédicale, CEA, Fontenay aux Roses, France.

swelling and degeneration in neurons of transgenic mice (18,19). The mechanisms that regulate SOD1 mitochondrial import are complex and involve the redox state of the cell, the intracellular distribution of the copper chaperone for SOD1 (CCS), and the folding of SOD1 (20). Indeed, increased localization of mutant SOD1 in mitochondria induced by CCS overexpression in mice causes early loss of mitochondrial function and accelerates the disease course (23).

Despite the evidence that a portion of mutant SOD1 localizes to mitochondria, it still remains to be proven that it causes mitochondrial dysfunction directly. A large amount of mitochondrial SOD1 is concentrated in the intermembrane space (IMS) (5,14,15,19–21). Therefore, in this study we have evaluated the impact of wild-type (WT) or two mutant SOD1 (G93A and G85R) targeted to the IMS on neuronal survival, mitochondrial bioenergetics, mitochondrial dynamics, and neuritic outgrowth of motor neuronal cells, and compared it with the effects of the corresponding untargeted (canonical) forms of SOD1. We demonstrate that mutant SOD1 localized in the IMS causes neuronal toxicity and abnormalities in mitochondrial morphology and dynamics, indicating that mutant SOD1 accumulated in mitochondria contributes to disease pathogenesis.

RESULTS

Targeting of SOD1 to the mitochondrial IMS in motor neuronal NSC34 cells

To direct the import of hSOD1 to the mitochondrial IMS we constructed fusion proteins consisting of WT or mutant (G93A or G85R) hSOD1 appended in-frame at their N-terminus to the mitochondrial import signal of *Saccharomyces cerevisiae* cytochrome b2 (CytB2). The CytB2 targeting peptide is comprised of 80 amino acids: the first 31 direct the import into the mitochondrial matrix, where they are cleaved by matrix metalloproteases (MMP), whereas the remaining 49 amino acids direct the export of the resulting peptide to the IMS, where they are cleaved by the intermembrane space proteases (IMP) (24). In our final construct, we added four residues corresponding to the mature CytB2 to the N-terminus of SOD1 to ensure proper recognition by IMP (Fig. 1A).

We first characterized the subcellular localization of different WT and two mutant IMS hSOD1 in transiently transfected COS cells by confocal microscopy, and demonstrated targeting to the mitochondria, as indicated by colocalization with the mitochondrial dye Mitotracker Red (Fig. 1B). In contrast, untargeted WT or mutant hSOD1 appeared diffusely distributed in the cytosol, with limited colocalization with mitochondria (not shown).

In order to study the effects of mitochondrial SOD1 in a disease-relevant cell line, we generated stably transfected NSC34 cells expressing IMS-targeted or untargeted SOD1. NSC34 is a hybrid motor neuron-like cell line produced by fusion of N2A neuroblastoma cells and embryonic mouse spinal cord neurons, which displays several typical properties of motor neurons (25,26). In cell homogenates from NSC34 cells expressing WT or G93A IMS-targeted hSOD1, western blot using a polyclonal anti-SOD1 antibody (Fig. 2A), that recognized both human and mouse SOD1 (mSOD1), indicated that, in addition to mature hSOD1 (M), there was a proportion of IMS-hSOD1 that was either uncleaved (i.e. full-length, P1) or only cleaved at the first site (i.e. −31 amino acids, P2). Enriched mitochondrial fractions showed the coexistence of all three products, P1, P2 and mature protein (Fig. 2B). The presence of IMS-targeted G85R hSOD1 in mitochondria was demonstrated using human-specific monoclonal antibodies (Fig. 2C, first lane), because this mutant co-migrates with mouse endogenous SOD1.

We took advantage of the known sensitivity of G85R SOD1 to proteinase K digestion (19) to investigate the intramitochondrial localization of IMS-hSOD1. To test for mitochondrial integrity, we used Hsp60, a matrix protein. Hsp60 was partially digested after proteinase K treatment (Fig. 2C, second lane), suggesting that mitochondrial membranes were partially permeant to proteinase K. Nevertheless, a portion of both P1 precursor and mature G85R peptides were protected from digestion, indicating that they were enclosed within intact mitochondrial membranes (Fig. 2C, second lane). Upon detergent solubilization, all of Hsp60 and most of the IMS-hSOD1 were digested (Fig. 2C, third lane). Upon hypo-osmotic swelling to rupture the outer membrane and allow the access of proteinase K to the IMS, all of IMS-targeted G85R hSOD1 was digested, whereas the matrix protein Hsp60 was partially preserved (Fig. 2D). Since virtually no hSOD1 was resistant to proteinase K digestion, we concluded that no hSOD1 accumulated into the mitochondrial matrix (Fig. 2D).

Native gel SOD1 activity assays in isolated mitochondria showed that both IMS-targeted WT and G93A hSOD1 displayed increased enzymatic activity as compared with mock-transfected cells (Fig. 2E), whereas mitochondria expressing IMS-G85R hSOD1 did not show increased activity, because this mutant is inactive (27).

Because we wanted to compare the effects of IMS-targeted with those of untargeted mutant SOD1, NSC34 cells were also stably transfected with canonical WT or mutant hSOD1. By cell fractionation and western blot analyses, hSOD1 was found in both cytosolic and mitochondrial fractions of cells transfected with WT, G93A and G85R (data not shown).

We also wanted to ensure that recombinant hSOD1 was mostly localized in mitochondria and not in the cytosol in IMS-hSOD1 expressing cells. Typical mitochondria isolation methods are not completely appropriate for this purpose, because some mitochondria are prone to break and release IMS-hSOD1 to the cytosol (data not shown). Therefore, we treated hSOD1 expressing cells with digitonin under conditions that permeabilize the plasma membrane and not the outer mitochondrial membrane. As shown in Figure 2F, Akt shifted from the pellet fraction to the supernatant fraction upon digitonin treatment and centrifugation; although cytochrome c remained in the pellet fraction. Untargeted hSOD1 was largely released to the supernatant after digitonin treatment (Fig. 2F), which indicated that it was mainly localized in the cytosol. Instead, WT IMS-hSOD1 was retained in the pellet, demonstrating that it was mainly localized in the mitochondria. Longer exposure of the same blots revealed that a very small amount of IMS-hSOD1 (estimated to be $<1\%$) was in the cytosol (Fig. 2F). The mitochondrial localization

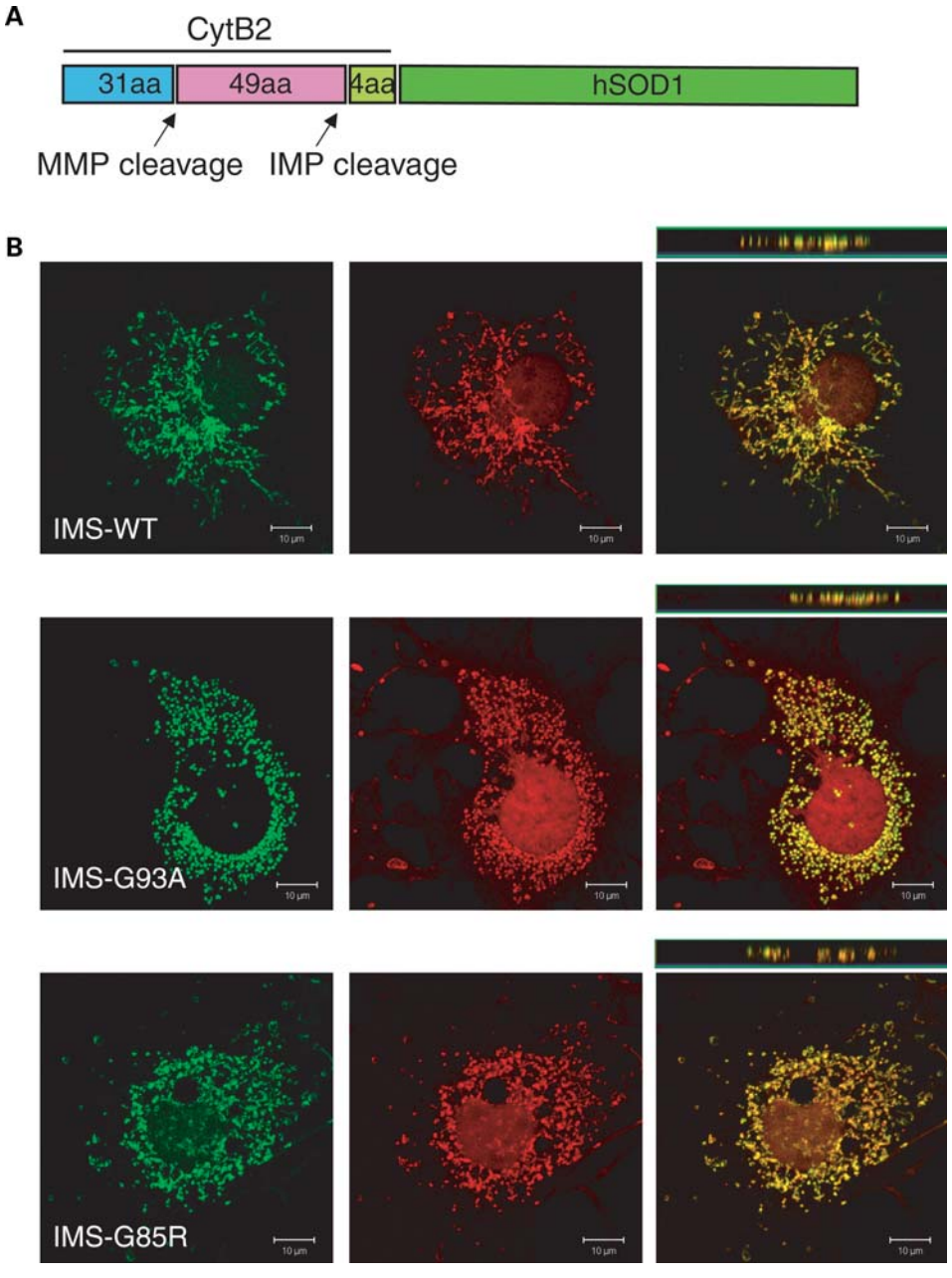

Figure 1. Targeting of SOD1 to mitochondria in cultured cells. (**A**) Schematic representation of the fusion protein containing human SOD1 (hSOD1) appended in-frame at its N-terminus to the mitochondrial import signal of cytochrome b2 (CytB2). MMP, matrix metalloproteases; IMP, intermembrane space proteases. (**B**) Transient transfection of WT or mutant (G93A and G85R) IMS-hSOD1 in COS cells. Recombinant SOD1 is immuno-labeled in green and mitochondria stained with the fluorescent dye Mitotracker red. The overlay of the two images indicates that IMS-h SOD1 localizes within mitochondria. Colocalization of the two fluorochromes is further confirmed by z-section reconstruction (insets).

of G93A and G85R mutant IMS-targeted hSOD1 was similar to WT (data not shown).

IMS-targeted mutant hSOD1 increases susceptibility to cellular stress

We compared the effects of constitutively expressing IMS-targeted or untargeted hSOD1 in NSC34 cells by assessing cell toxicity. Under normal growth conditions, there was no difference in viability and cell morphology between cells expressing hSOD1 and mock-transfected cells. Untreated cells expressing either WT or mutant IMS-hSOD1 had round morphology and similar diameters, as shown in the representative micrographs of NSC34 cells, in Figure 3A (top panels). Moreover, mitochondrial ATP synthesis, cytochrome c oxidase, and citrate synthase activities were unchanged in cells expressing either IMS-targeted or canonical mutant and WT hSOD1, as compared with mock-transfected cells (data not shown). We then subjected cells to modified conditions that induce metabolic stress. First, we tested the ability of

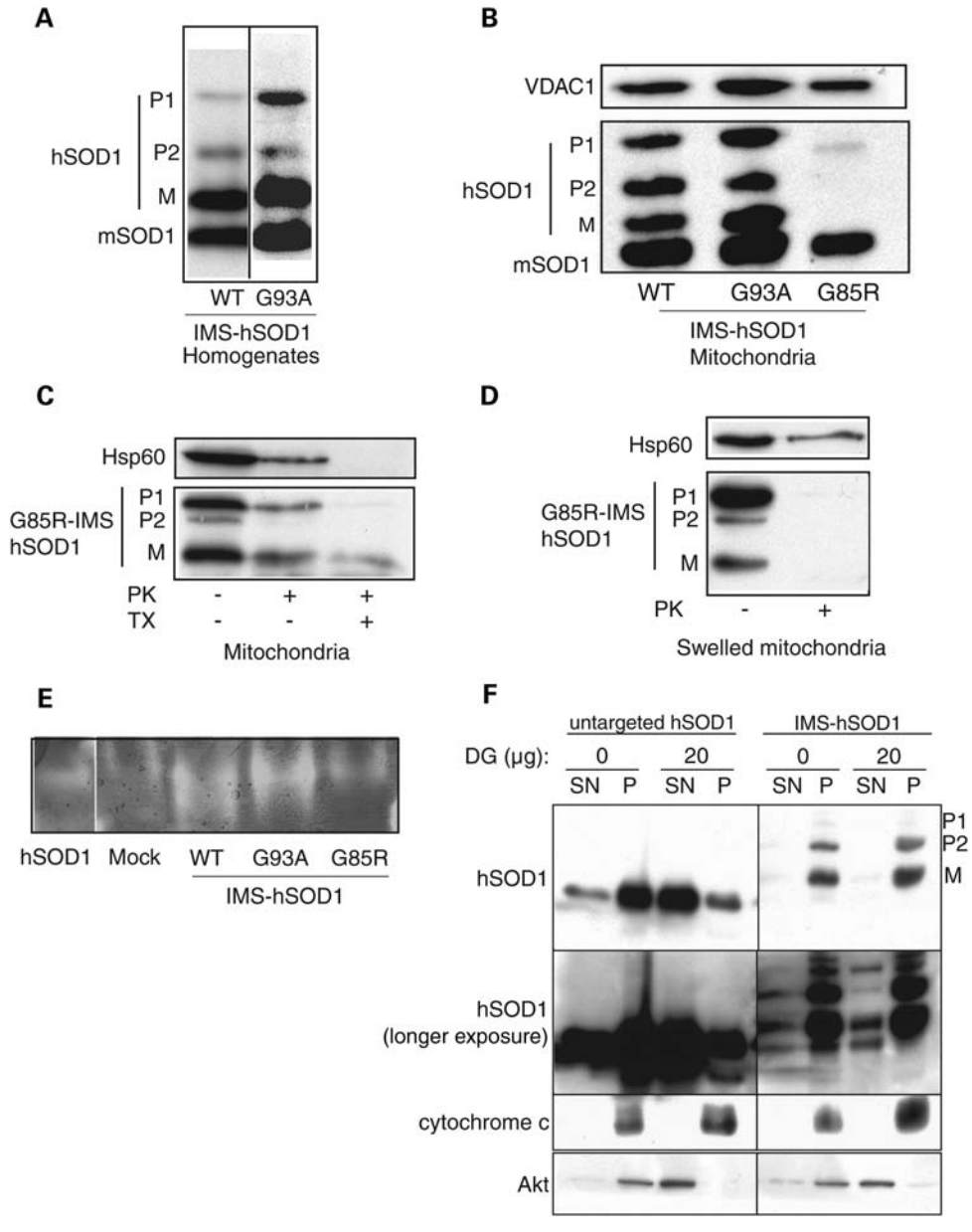

Figure 2. Expression and localization of IMS-targeted hSOD1 in NSC34 cells. (**A**) Western blot of cellular homogenates from cells stably expressing WT and G93A IMS-hSOD1 using a polyclonal anti-SOD1 antibody that recognizes both the human and the mouse protein. mSOD1, mouse SOD1; P1 and P2, precursor products of incomplete protein cleavage; M, mature, fully processed hSOD1. (**B**) Western blot of enriched mitochondrial fractions from NSC34 cells stably transfected with WT or mutant IMS-hSOD1. Each lane contains 50 μg of protein. The mitochondrial outer membrane protein VDAC1 is used as a loading control. Note that mature G85R mutant IMS-hSOD1 is masked by endogenous mSOD1. (**C**) Western blot of mitochondria from cells stably expressing G85R IMS-hSOD1 using a human specific anti-SOD1 antibody (first lane). Proteinase K (PK) treatment does not completely digest mutant hSOD1 (second lane), but digestion is almost complete when mitochondrial membranes are solubilized with detergents (TX, third lane). (**D**) Western blot of mitochondria form G85R IMS-hSOD1 cells after hypo-osmotic swelling. PK treatment fully digested mutant hSOD1 only when the outer mitochondrial membrane was disrupted. (**E**) SOD1 native activity gel assay of enriched mitochondrial fractions from cells stably expressing IMS-hSOD1. hSOD1, purified human SOD1; mock, cells transfected with empty plasmid. (**F**) Western blot of supernatant (SN) and pellet (P) fractions of cells expressing WT untargeted or IMS-hSOD1 after digitonin (DG) treatment. A human specific anti-SOD1 antibody demonstrates the presence of hSOD1 only in the pellet fraction of cells expressing IMS-hSOD1. Longer exposure of the same blot shows small amounts of hSOD1 in the supernatant after DG treatment when IMS-hSOD1 is expressed. Cytochrome c and Akt antibodies are used as controls for IMS and soluble cytosolic protein fractions, respectively.

these cells to grow either in medium lacking glucose and containing pyruvate and galactose to force ATP synthesis from oxidative metabolism (5), or in conditions of serum deprivation. Regardless of hSOD1 expression, cells exposed to galactose medium slowed their replication rate and presented some morphological changes, characterized by enlargement and flattening of the cell body and extrusion of cell processes, similar to neurites (Fig. 3A, bottom panels).

Cell death was assayed by lactate deshydrogenase (LDH) release after 72 h of growth in pyruvate/galactose or in

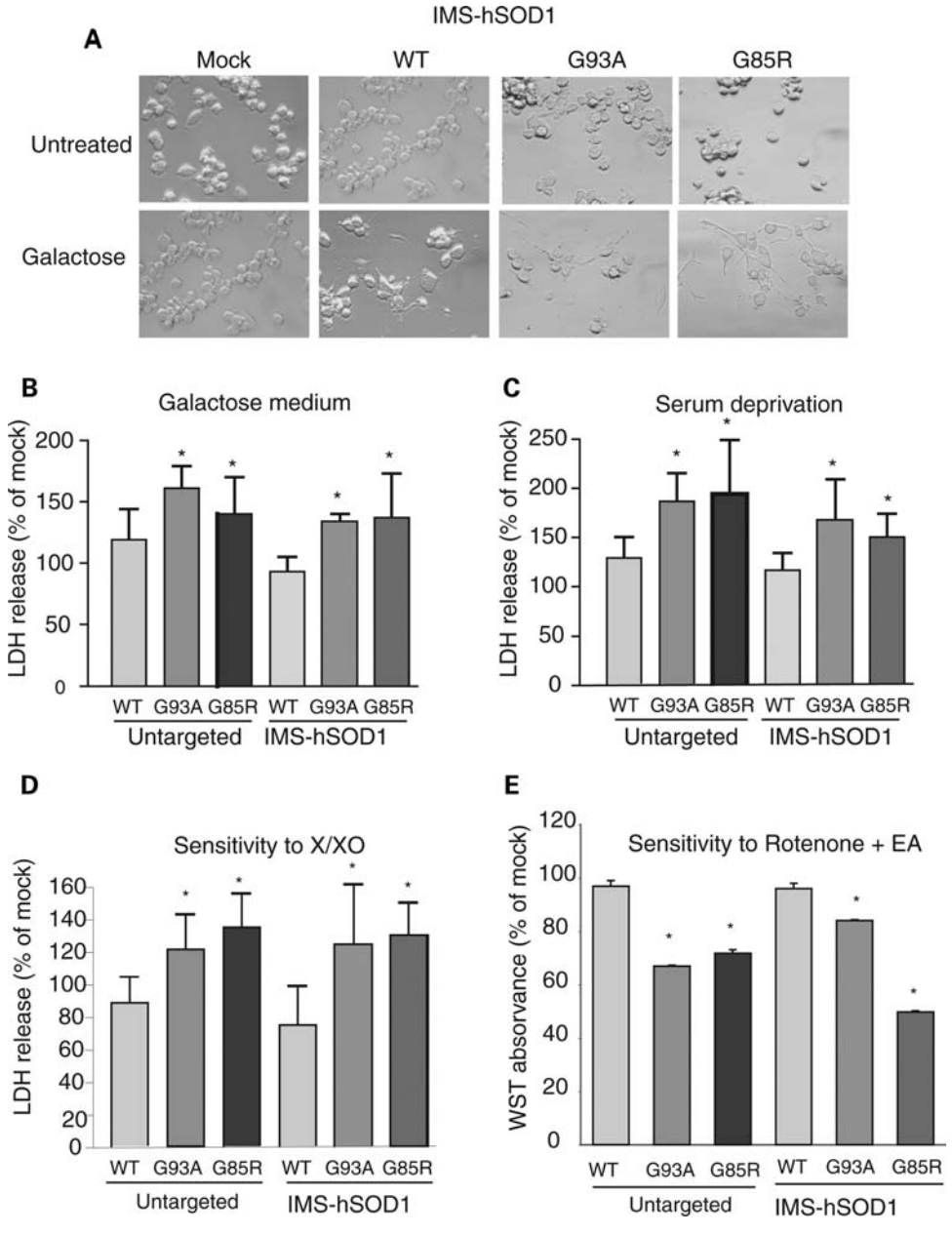

Figure 3. Metabolic stress in NSC34 cells expressing IMS-targeted hSOD1. (**A**) Representative phase contrast micrographs of NSC34 cells either mock transfected or stably expressing IMS-targeted hSOD1. Untreated, normal growth conditions; galactose, galactose medium induces morphologic changes in all cells, including extrusion of cell processes, similar to neurites (arrows). (**B, C, D**) Quantification of cell death by LDH release in cells grown in galactose medium ($n = 7$), serum-deprived medium ($n = 8$) and xantine oxidase (X/XO) medium ($n = 8$). (**E**) Cell viability by WST-1 assay ($n = 8$) in cells treated with the combination of rotenone (50 nM) for 72 h, plus ethacrynic acid (100 μM). $^{*}P < 0.05$ compared with mock-transfected controls. Error bars represent the SEM.

serum-deprived medium. Under these metabolic stressors, LDH release was highest in cells expressing either untargeted or IMS-targeted mutant hSOD1, whereas WT hSOD1 expression did not significantly affect cell viability, as compared with control mock-transfected cells (Fig. 3B). Loss of viability in cells expressing mutant hSOD1 exposed to either galactose or lack of serum was confirmed by MTT assay (data not shown). These results suggest that IMS-targeted mutant hSOD1 is capable of sensitizing neuronal cells to metabolic stress.

We also tested the sensitivity of mutant hSOD1 cells to oxidative stress. We first induced ROS production by adding a combination of xantine and xantine-oxidase (X/XO) in the growth medium (28). Exposure to X/XO for 6 h significantly increased toxicity in cells expressing either IMS-targeted or untargeted mutant hSOD1, as measured by LDH (Fig. 3D) and by MTT assays (data not shown). We then treated cells for 72 h with the complex I inhibitor rotenone with the addition of the gluthatione depleting agent ethacrynic acid (EA) during the last 16 h of rotenone treatment. We determined

that 100 μM EA for 16 h does not result in cell death in untransfected NSC-34 cells, but longer treatments cause cell death regardless of SOD1 expression (data not shown). Because in cultured cells rotenone at high doses may exert toxic effects independent of mitochondrial dysfunction (29), we used a low concentration (50 nM) that is not lethal to cells, when administered in the absence EA, but causes an increase in ROS production from complex I of the respiratory chain (29). The combination of rotenone and EA resulted in loss of cell viability, as determined by WST-1 assay, in cells expressing IMS-targeted or untargeted mutant hSOD1 (Fig. 3E). These results suggest that mitochondrial accumulation of mutant SOD1 is responsible for the increased sensitivity of neuronal cells to oxidative stress.

IMS-targeted mutant hSOD1 causes mitochondrial morphological changes in differentiated NSC34 cells

Mutant SOD1 causes mitochondrial abnormalities in ALS patients (11) and transgenic mouse models (9,10,18,30). Furthermore, reduction of average mitochondrial length (i.e. mitochondrial fragmentation) has been reported in motor neuron axons of transgenic SOD1 mutant mice (31). Mitochondrial fragmentation was also found in undifferentiated NSC34 cells expressing mutant SOD1 (8,32). However, undifferentiated NSC34 lack the principal structural features of motor neurons, because they are round and devoid of neurites. Therefore, we induced differentiation in NSC34 cells for 6 days, in differentiation medium, containing 1:1 DMEM/Ham's F12 supplemented with 1% fetal bovine serum (FBS), 1% P/S and 1% modified Eagle's medium non-essential amino acids, followed by transfection with mitoGFP (i.e. GFP targeted to the mitochondrial matrix) and imaging 36 h post-transfection. Individual mitochondria could be easily identified in neurites (Fig. 4A). Mitochondria were homogeneously distributed along neurites with occasional clustering, which in the case of IMS-targeted G85R hSOD1 expressing cells was markedly increased as compared with mock-transfected cells, affecting ~60% of neurites (Fig. 4B). The average mitochondrial length in neurites was significantly reduced in cells expressing IMS-targeted or untargeted mutant SOD1, as compared with controls (Fig. 4C), indicating mitochondrial fragmentation. The density of mitochondria in neurites was calculated as the average length of all the mitochondria contained within a 50 μm neuritic segment. Mitochondrial density was decreased in cells expressing both IMS-targeted mutant hSOD1 forms, whereas only G93A mutant untargeted hSOD1 showed decreased density, as compared with controls (Fig. 4D). The decrease in density reflects the smaller size of mitochondria, which is not balanced by an increase in the number of mitochondria. This abnormality is specific to differentiated cells, because undifferentiated mutant hSOD1 cells did not have a reduction in mitochondrial mass, as evidenced by normal content of mitochondrial enzymes (data not shown). Average mitochondrial length was also significantly reduced in the soma of differentiated cells expressing both IMS-targeted mutant hSOD1 forms, whereas only G93A mutant untargeted hSOD1 showed decreased mitochondrial length (Fig. 4E).

Mitochondrial dynamics in neurites are abnormal in differentiated IMS-targeted mutant SOD1 expressing NSC34 cells

Mutant SOD1 causes an impairment of mitochondrial axonal transport in primary cultured neurons (31). To assess whether IMS-targeted mutant SOD1 is capable of disrupting mitochondrial neurite transport, NSC34 cells were induced to differentiate and transfected with mitoGFP as described above. Mitochondrial transport along neuritic processes was measured by time-lapse *in vivo* microscopy. Kymographs obtained from the recorded movies (Fig. 5A) were used for quantification of the proportion of moving mitochondria in each direction (anterograde and retrograde). Approximately 37% of all mitochondria were mobile during the course of the recording (5 min). The proportion of mobile mitochondria was unchanged in NSC34 cells expressing untargeted or IMS-targeted WT hSOD1, whereas both untargeted and IMS-targeted G93A and G85R mutant hSOD1 caused a significant reduction of mobile mitochondria (Fig. 5B and C). Mitochondrial anterograde and retrograde transport were equally affected in untargeted or IMS-targeted hSOD1 mutant cells. Note that in Figure 5C and D the sum of anterograde plus retrograde mitochondrial movements is slightly higher than the total, because mitochondria that moved bi-directionally in the course of the recording were counted in both groups.

These results indicate that the presence of mutant hSOD1 in the IMS is sufficient to cause mitochondrial transport defects, which may contribute to the functional and morphological mitochondrial abnormalities observed in differentiated mutant SOD1 NSC34 cells.

IMS-targeted mutant hSOD1 impairs neurite maintenance in differentiated NSC34 cells

To assess the consequences of impaired mitochondrial morphology and dynamics on the fate of the neurite, NSC34 cells were induced to differentiate for 8 or 12 days prior to morphometric analyses of neurite length. The panels in Figure 6A are representative of the various NSC34 lines after 12 days of differentiation. Approximately 30% of the cells projected neurites of various lengths and there was no difference in the number of differentiated cells or in the average neurite length (40.1 μm ± 1.6) after 8 days among the lines (data not shown). The increase in average neurite length between days 8 and 12 was used as a measure of neurite viability. The average neurite length increased by ~10 μm in mock-transfected and WT hSOD1-expressing cells. However, in IMS-targeted mutant hSOD1-expressing cells the average neurite length decreased by day 12 and was significantly shorter than in mock-transfected and IMS-targeted WT hSOD1 cells (Fig. 6B). Neurites of cells expressing untargeted mutant hSOD1 were not significantly shorter than controls.

These data suggest that IMS-targeted mutant SOD1 impairs the maintenance of viable neuronal processes by disrupting the dynamics of the axonal mitochondrial network.

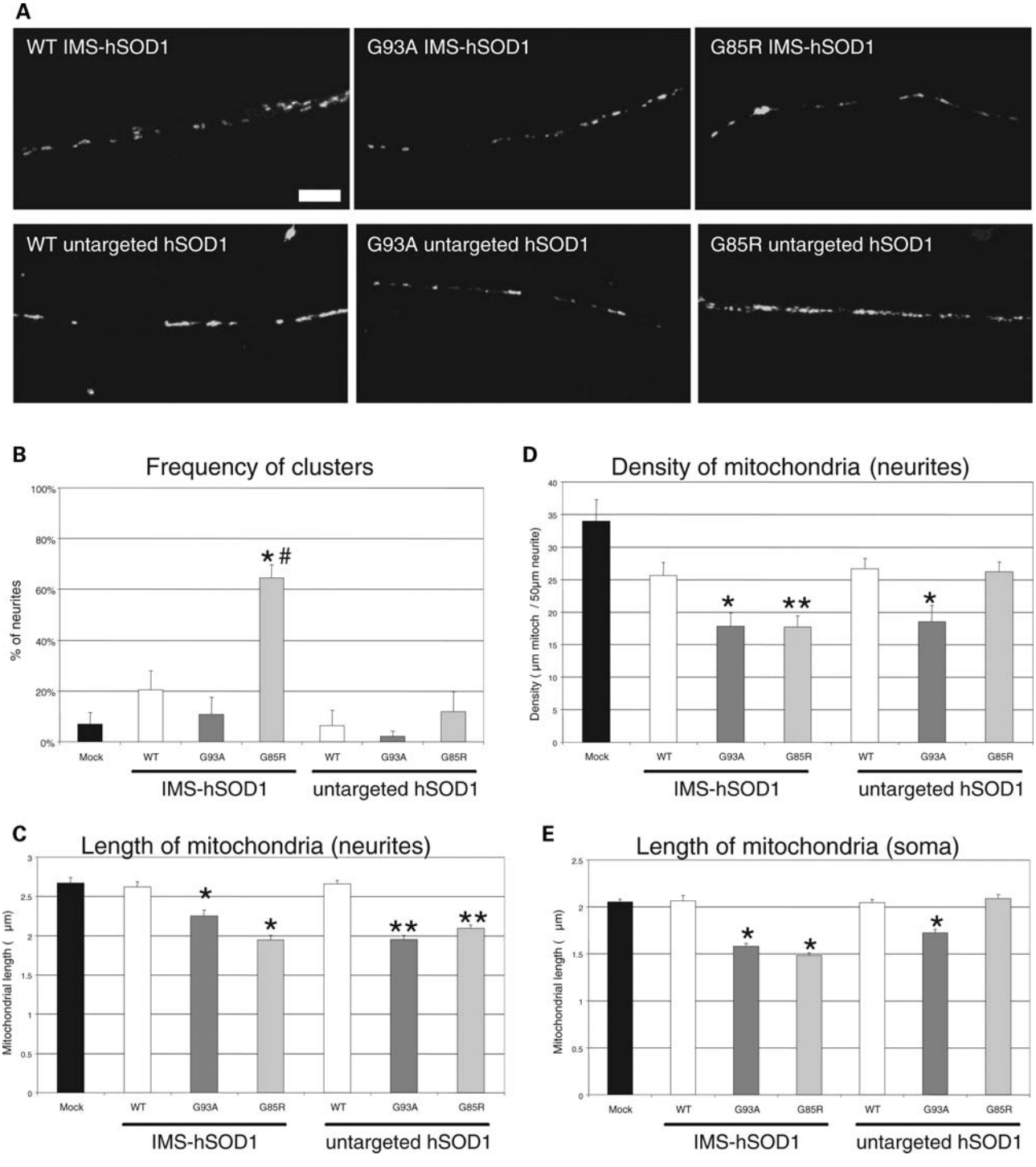

Figure 4. Mitochondrial abnormalities in neurites of differentiated mutant hSOD1 motor neuronal cells. (**A**) Representative images of mitochondria along neurites in differentiated NSC34 clones stably expressing IMS- or untargeted hSOD1. Mitochondria are identified by mitoGFP labeling. Note a cluster of mitochondria in G85R IMS-hSOD1 neurite. Scale bar, 10 µm. (**B**) Clustering of mitochondria in neurites. n (neurites) = 20–50 from three to six independent experiments. $^{*}P < 0.005$ versus WT IMS-hSOD1; $\#P < 0.00005$ versus mock. Error bars represent the SEM. (**C**) Size (length) and (**D**) density (mass per neurite segment) of mitochondria was quantified in neuritic segments. Data were referred to an arbitrary 50 µM segment. From 17 to 45 neurites were analyzed in three to four independent experiments. n (mitochondria) = 223–754. $^{*}P < 0.0005$ versus WT-IMS; $^{**}P < 0.\ 05 \times 10^{-4}$ versus WT. (**E**) Length of mitochondria in the cell bodies of differentiated NSC34 cells. From 16 to 18 somas were analyzed in three independent experiments. $^{*}P < 0.05 \times 10^{-8}$ versus mock controls.

DISCUSSION

In recent years, several reports have identified the presence of a proportion of SOD1 in mitochondria of mammalian cells. Concomitantly, it was also reported that mutant SOD1 results in mitochondrial dysfunction, which might contribute to motor neuron toxicity (2,33). However, because mutant SOD1 is widely distributed throughout the cell in the

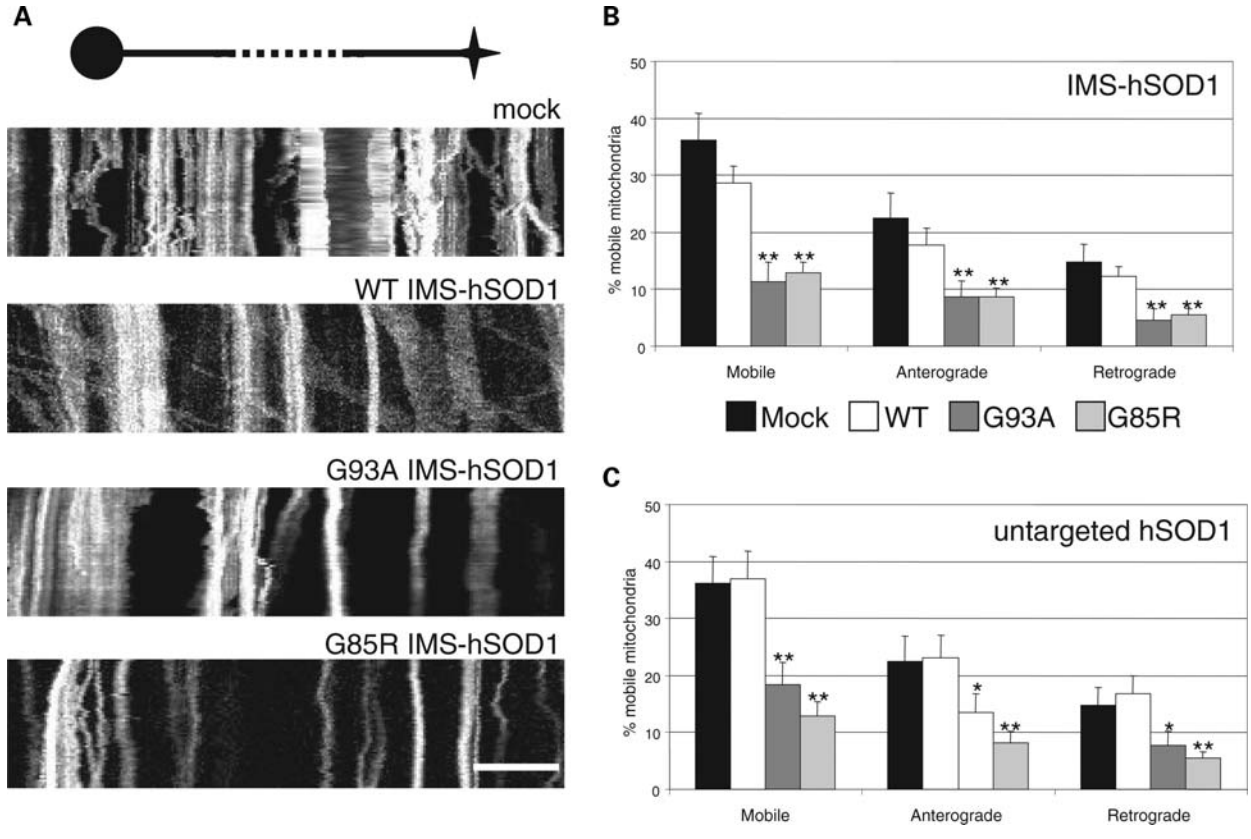

Figure 5. Altered mitochondrial dynamics in differentiated mutant SOD1 NSC34 cells. (**A**) Representative kymographs of mitoGFP-labeled mitochondria from control (mock and WT IMS-hSOD1) and mutant (G93A and G85R IMS-hSOD1) cells. Total imaging time, 5 min. Scale bar in all panels, 10 μm. Note the reduced motility in mutant SOD1 cells indicated by a prevalence of vertical fluorescent lines corresponding to immobile mitochondria. (**B**) Relative motility of neuritic mitochondria from IMS-hSOD1 cells. $n = 10-13$ neurites, $^{*}P < 0.05$, $^{**}P < 0.005$ referred to mock-transfected cells. (**C**) Relative motility of neurite mitochondria in untargeted hSOD1 cells. $n = 9-13$ neurites, $^{*}P < 0.05$, $^{**}P < 0.005$ referred to mock control cells. Error bars represent the SEM.

cytoplasm and in various other organelles, the question of whether the mitochondrial component is the cause of mitochondrial dysfunction and neuronal toxicity remains to be directly addressed. Furthermore, since mutant SOD1 is likely to have multiple toxicity sites outside of the mitochondria, including the proteasome, the endoplasmic reticulum, the cytoskeleton and many others (34), the relative role of mitochondrial impairment deriving from mutant SOD1 in the mitochondria in disease pathogenesis remains to be elucidated.

In this work, we have investigated the effects of targeting mutant hSOD1 to the IMS of mitochondria, in cultured NSC34 motor neuron cells. Our main goal was to provide a proof of principle that the mitochondrial localization of mutant SOD1 can cause mitochondria toxicity *per se*. We chose to target mutant hSOD1 to the IMS because, despite the fact that we have identified a portion of mitochondrial SOD1 associated with the inner membrane on the matrix side (19), there is general agreement that a large amount of SOD1 resides in the IMS (15,20).

We reasoned that if the mitochondrial component of mutant SOD1 is implicated in ALS pathogenesis, the expression of an IMS-targeted mutant SOD1 should cause mitochondrial dysfunction and cell toxicity. Here, we first demonstrated that IMS-targeted hSOD1 retains enzymatic activity, suggesting that this recombinant protein can be folded and metallated. Then, we showed that two different mutant hSOD1 targeted to the IMS cause mitochondrial distress. Both untargeted and IMS-targeted mutant hSOD1 did not cause toxicity or mitochondrial dysfunction, when cells were cultured under standard conditions, which suggests that actively replicating cells are resistant to mutant SOD1 toxicity or that selected cells have adapted to constitutive expression of mutant SOD1. In agreement with this observation, several reports have described that immortalized neuronal cells are resistant to mutant SOD1 toxicity, and that metabolic stress needs to be applied to detect a pathologic phenotype (8,28,35). However, Ferri and colleagues have shown lack of mutant SOD1 toxicity under normal growth conditions in NSC34 cells with inducible protein expression (36). In a later report, the same group has used an inducible system to deliver G93A mutant SOD1 to the mitochondrial IMS by appending the cytochrome C1 N-terminal sequence. They found that 48 h after induction there was increased caspase 3 activation and loss of cell viability, suggesting that inducible mutant SOD1 targeted to mitochondria may be more cytotoxic than the untargeted protein (37).

In our system, we used various approaches to cause metabolic stress, including oxidative stress from exogenous (with X/XO) or endogenous (with rotenone) sources, and galactose medium to force oxidative phosphorylation. Importantly, the

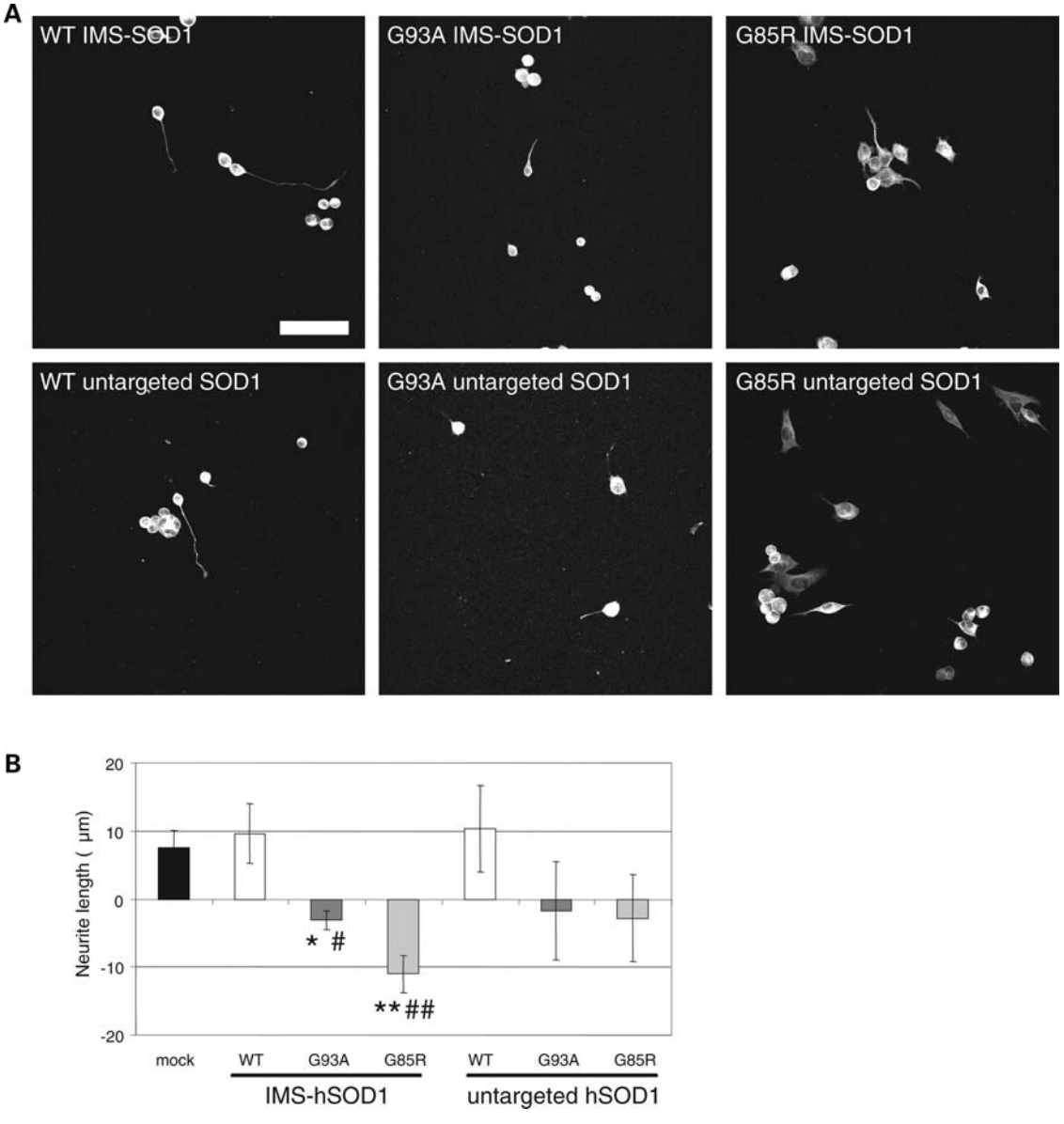

Figure 6. Targeting of mutant SOD1 to mitochondria causes a failure in neurite maintenance. (**A**) Representative images of NSC34 cells after 12 days in differentiation medium. Neurites are labeled using a MAP2 antibody. Scale bar, 50 μm. (**B**) Quantification of neurite length plotted as the average change between day 8 and day 12 after inducing differentiation. n (neurites at 8/12 days) = 52–346 from three independent experiments. $^{*}P < 0.0005$ and $^{**}P < 0.000005$ versus mock; $\#P < 0.05$ and $\#\#P < 0.0005$ versus WT IMS-SOD1. Error bars represent the SEM.

expression of WT IMS-SOD1 did not affect cell viability under any of these stress conditions. Instead, all of these stressors caused death in NSC34 cells containing mutant IMS-SOD1.

The mechanisms whereby mutant SOD1 in mitochondria sensitizes cells to stress remains to be further elucidated, but a combination of different factors is likely. Mutant SOD1 has been proposed to promote aberrant chemistry and enhance the production of highly reactive peroxynitrate in the presence of superoxide and nitric oxide (38). Both superoxide and nitric oxide are produced in mitochondria, where they can interact with mutant SOD1 in the IMS. In line with this interpretation, nitrated and aggregated proteins, including respiratory chain subunits, have been shown to accumulate in spinal cord mitochondria from mutant SOD1 transgenic mice (39). Another potential mechanism of SOD1 toxicity in mitochondria, which may be activated by changes in redox state, is the aggregation of the mutant protein, either with itself to form homo-oligomers or with other mitochondrial proteins (19,36,40–42). Interestingly, disulfide-linked SOD1 oligomers were associated with cytotoxicity in the inducible mutant mitochondrial SOD1 model (37).

Mutant SOD1 may interact with proteins involved in the maintenance of mitochondrial structure and dynamics (3,43), resulting in abnormalities of the mitochondrial network and impairment of mitochondrial transport. It was shown that mitochondria of undifferentiated NSC34 cells expressing mutant SOD1 develop aberrant morphology characterized by

abnormal cristae and fragmented network (32). Furthermore, impaired mitochondrial axonal transport was demonstrated in cultured motor neurons from SOD1 mutant rodents (31).

Taking advantage of the potential of NSC34 cells to differentiate, we investigated for the first time the effects of IMS-targeted mutant SOD1 on mitochondrial transport and morphology in neuritic processes. Mutant IMS-SOD1 impairs mitochondrial motility both in anterograde and retrograde directions, resulting in organelle fragmentation and decreased density of mitochondria along neurites. Impaired mitochondrial transport was associated with inability to maintain viable neurites, as demonstrated by neuritic shortening over time. These observations are consistent with the notion that SOD1 familial ALS develops as a dying-back neuropathy that initiates and progresses from the distal to the proximal portions of the motor neuron (44), and causes paralysis even in the absence of cell body degeneration in the spinal cord (10).

Mitochondrial transport abnormalities can result in failure of mitochondria originated in the cell body to reach the synaptic terminals and altered retrograde transport of mitochondria from the periphery to the cell body for degradation. Mitochondrial transport abnormalities may be critical in motor neurons, where cellular components have to move long distances throughout axons, and may contribute to explain the selective degeneration of MN in ALS (3). The mechanisms whereby mutant IMS-SOD1 impairs mitochondrial axonal dynamics remain to be elucidated, but they are likely to involve defective mitochondrial bioenergetics and aberrant interactions with the machinery that regulates mitochondrial dynamics (3).

Further *in vivo* studies in transgenic mouse models expressing IMS-targeted mutant SOD1 are warranted for the future. Nevertheless, our observations in motor neuronal cells strongly support the role of mutant SOD1 localized in the IMS in causing mitochondrial dysfunction and neuronal degeneration in familial ALS.

MATERIALS AND METHODS

Plasmids

WT and G93A or G85R mutant forms of hSOD1 were cloned at the *BamH*I site of the mammalian expression vector pIRESNeo3 (Clontech, Mountain View, CA, USA). To target SOD1 to the mitochondrial IMS, we used a cDNA encoding the first 84 amino acid of the *S. cerevisiae* CytB2, which contains the mitochondrial targeting sequence, plus four amino acids of the mature protein (provided by Dr Carla Koheler, University of California, Los Angeles, CA, USA). CytB2 was cloned into pIRESNeo3 at the *BamH*I site, and then the cDNA encoding for either WT or mutant SOD1 was cloned in-frame with the C-terminus of the CytB2 pre-sequence using *Not*I and *BstX*I sites generated by PCR. The final construct was confirmed by DNA sequencing. A mitoGFP construct with targeted expression of GFP to the mitochondrial matrix (45) was used for labeling of mitochondria in morphology and transport studies.

Cell culture and transfection

COS cells (from ATCC, American Type Culture Collection, Manassas, VA, USA) were maintained in Dulbecco's modified Eagle's medium (DMEM, Invitrogen, Carlsbad, CA, USA) supplemented with 5% v/v FBS and 1% antibiotic anti-mycotic solution (Invitrogen). The motor neuron-like cell line NSC34 (provided by Dr Neil Cashman, University of Toronto, Toronto, ON, Canada) were maintained in DMEM supplemented with 10% v/v FBS and 1% antibiotic anti-mycotic solution. When differentiation was required, cells were plated onto poly-D-lysine-coated plates and grown in differentiation medium, which contains 1:1 DMEM/Ham's F12 (Invitrogen) supplemented with 1% FBS, 1% P/S and 1% modified Eagle's medium non-essential amino acids (Invitrogen).

Transient transfections of COS cells were performed with 3 μl of the FuGENE 6 transfection reagent (Roche, Indianapolis, IN, USA) mixed with 1 μg of plasmid DNA, as recommended by the manufacturer. For the generation of stable cell lines expressing SOD1 constructs, NSC34 cells were transfected as above, and after 24 h selection was started with 500 μg/ml of the neomycin analog G418 (Invitrogen). G418-selected cells were constantly maintained in the presence of the selective drug. For live-cell imaging studies on differentiated cells, NSC34 motor neurons were subjected to differentiation medium for 6 days, and then transfected with 0.75 μg mitoGFP and 1 μl of Lipofectamine 2000 (Invitrogen) and analyzed 36 h later.

ATP synthesis

Mitochondrial ATP synthesis was measured in digitonin permeabilized NSC34 cells, using a luciferase/luciferin based kinetic assay, as previously described, with malate and pyruvate as respiratory chain substrates (46).

Mitochondrial isolation from cultured cells

NSC34 cells stably expressing hSOD1 constructs were washed with PBS, trypsinized, and resuspended in 10 ml of cold NKM buffer (130 mM NaCl, 5 mM KCl, 7.5 mM $MgCl_2$) containing 1 mM DTT and a cocktail of protease inhibitors (Sigma, Saint Louis, MO, USA). Cells were then centrifuged at 3000*g* for 3 min at 4°C and the resulting cell pellet was resuspended in 3 ml of RSB buffer (10 mM Tris–HCl pH 7.6, 10 mM KCl, 0.15 mM $MgCl_2$, 1 mM DTT and PI), incubated 4 min on ice, and homogenized in glass–glass Potter–Elvehjem style homogenizer (pestle B) on ice. Then, 0.5 ml of 2 M sucrose was added and the homogenates were centrifuged at 600*g* for 10 min at 4°C. The resulting supernatants were centrifuged at 15 000*g* for 15 min at 4°C. The crude mitochondrial pellet was incubated with 150 mM KCl for 5 min on ice and centrifuged at 15 000*g* for 15 min at 4°C. The washed mitochondrial pellet was resuspended in 125 μl of chilled buffer containing 250 mM sucrose, 10 mM Tris–HCl, 10 mM EDTA 1 mM DTT and PI. Sample aliquots were snap-frozen in liquid nitrogen and stored at −80°C. Protein concentration in the samples were determined by a colorimetric assay (BioRad DC, Hercules, CA, USA).

Immunofluorescence and mitochondrial labeling

For immunocytochemistry, COS cells were transiently transfected on glass slides with untargeted or IMS-targeted WT,

G93A and G85R SOD1 constructs. After 48 h, cells were incubated for 30 min with 250 nM of the mitochondrial-specific fluorescent dye MitoTracker Red (Invitrogen). Cells were then fixed in a 4% paraformaldehyde solution, permeabilized with 0.1% Triton-X100, and immunostained with mouse monoclonal anti-SOD1 antibodies (Santa Cruz Biotechnology, Santa Cruz, CA, USA). Secondary Cy2-conjugated anti-mouse IgG (Jackson Immunochemicals, West Grove, PA, USA) were used for fluorescence visualization.

Differentiated NSC34 cells stably expressing SOD1 proteins were transfected with mitoGFP to label mitochondria, and fixed and immunostained with antibodies against and MAP2 (Chemicon, Temecula, CA, USA) to reveal the entire neurite length. Images were collected using a Leica SP5 spectral confocal microscope (Leica Microsystems Inc, Bannockburn, IL, USA) equipped with a HCX PL APO CS 63×/NA1.4 oil objective, and optical sections were acquired every 0.5 μm and standard pinhole of 1 AU to achieve high resolution of mitochondria.

SOD1 immunodetection

For western blots, cytosolic and mitochondrial fractions from NSC34 cells were separated by 12% SDS-PAGE and immunoblotted onto PVDF membranes (BioRad). Immunoreactive bands were detected with polyclonal antibodies that recognize both human and mSOD1 (Calbiochem, San Diego, CA, USA) or monoclonal antibodies (Santa Cruz Biotechnology) against hSOD1.

For assays of protease protection of mitochondrial proteins, isolated mitochondria from NSC34 cells expressing IMS-targeted G85R hSOD1 were treated with 20 μg/ml proteinase K (Roche Applied Sciences, Indianapolis, IN, USA) on ice for 20 min either in the presence or the absence of 0.5% Triton-X100, as described (19). After inactivation of proteinase K with PMSF, the residual content of mitochondrial proteins was analyzed by western blot using specific antibodies. Alternatively, mitochondria were treated with hypotonic buffer (1 mM Tris–HCl) to swell and rupture the outer membrane and allow proteinase K to access the IMS.

To confirm the enrichment of SOD1 in mitochondria, 1 million cells were treated with or without 20 μg digitonin (Sigma) for 1 min at room temperature. Supernatant (containing soluble proteins) and pellet (containing membrane-bound organelles, including mitochondria) fractions were then obtained by centrifugation at 22 000*g* for 15 min at 4°C.

Other antibodies were used against VDAC1 (Invitrogen), Hsp60 (Assay Designs, Ann Arbor, MI, USA), Akt (Santa Cruz Biotechnology) and cytochrome c (BD Biosciences, San Jose, CA, USA).

Stress treatments and cell viability assays

Stable NSC34 cell lines expressing untargeted or IMS-targeted hSOD1 were seeded onto 48-well plates at 12 500 cells/well. The next day, cells were subjected to the following stress conditions: culture medium deprived of FBS; culture medium with 5 mM galactose instead of glucose; and treatment with 50 nM rotenone (a respiratory chain complex I inhibitor) for 72 h plus depletion of glutathione stores with EA (100 μM), during the last 16 h of treatment. In these stress paradigms, cell viability was assessed after 72 h. In another set of experiments, 10 000 cells were seeded onto 12-well plates, and 200 μM xanthine plus 10 mU/ml xanthine oxidase (Sigma) were added the next day to produce exogenous superoxide; cell viability was assessed after 6 h.

To determine cell survival after exposure to oxidative and metabolic stressors, several assays were used. 3-(4,5-Dimethylthiazol-2-yl)-2,5-diphenyltetrazolium bromide (MTT, Sigma) assay was used following manufacture's instructions. Absorbance was measured in duplicates in a plate reader (Packard Instrument Company, Downers Grove, IL, USA) at 570 nm. Alternatively, a similar Cell Proliferation Reagent WST-1 assay (Roche) was used to measure cell viability, according to the manufacturer's protocol. LDH release into the culture media was measured with a Cytotoxicity Detection kit (Roche) according to the manufacturer's protocol. The value of released LDH is expressed as the proportion of total cellular LDH content measured after lysing the cells with 2% Triton X-100.

Analysis of mitochondrial morphology, density and clustering

Metamorph software (Universal Imaging) was used for quantitative analysis of mitochondria measurements. For morphological quantification in neurites, z-sections were merged (using maximal projection) and mitoGFP-labeled mitochondria marked by longitudinal regions covering their entire length (from tip to tip). In cell bodies, mitochondria length was measured in each z-section covering the entire soma. The total number of mitochondria analyzed ranged from 223 to 754 for each group. For density quantification, the length of the entire neurite immunostained with anti-MAP2 antibodies was measured, and the sum of all mitochondrial lengths was divided by neurite length and referred to an arbitrary 50 μm segment. Only neurites longer than 40 μm were analyzed. Clustering of mitochondria was defined as an accumulation of several mitochondria that cannot be measured individually, having the cluster an irregular shape (not tubular), and more than 2 μm thick and more than 5 μm long. The number of neurites analyzed ranged from 14 to 50 in each category. Three to six independent experiments were performed.

Live-cell imaging and analysis mitochondria dynamics

For time-lapse microscopy, images were collected using a Zeiss LSM510 Laser Scanning Confocal Microscope (Zeiss Microimaging, Thornwood, NY, USA) with a 63x lens. A fully equipped live imaging station (CTI-Controller 3700 and incubator S, Leica Microsystems) allowed for the control of CO_2 content, humidity and temperature of both the stage (through a heated stage; Heating Insert P, PeCon) and the air during the curse of the experiment. Preliminary observation of the cells with either epifluorescence or 488-nm laser was performed at low light/laser intensities to prevent photo-toxicity. We selected neurites from 4 to 5 differentiated mitoGFP-positive NSC34 cells for each experiment (3–4 independent experiments), and mitochondrial transport

was followed for 5 min with frames taken every 5 s. Pinhole opening was set at 2 AU.

We counted the number of mitochondria that presented retrograde or anterograde movements or remained stationary (293 for mock, 424 for WT, 222 for G93A, 402 for G85R; 183 for WT IMS, 130 for G93A IMS and 353 for G85R IMS). Movement was defined as changes in mitochondrion position in at least four consecutive time frames. A moving mitochondrion during the course of an experiment was scored as one movement event if no change in direction occurred; otherwise it was scored as $x + 1$ movements (where x is the number of changes in direction). Number of mobile mitochondria was referred to the total number of mitochondria present during the course of the experiment. Differences were measured by analysis of variance to compare mutant hSOD1 cells with WT hSOD1 and mock-transfected controls.

Analysis neurite length

To evaluate neurite maintenance over time in culture, 15 000 cells were plated on coated glass coverslips, and differentiation medium was added after 24–48 h. Cells were fixed 8 and 12 days later and stained with antibodies against MAP2 to label neurites. Only differentiated cells with one clearly defined neurite (no thread-like neurites, no multiple neurites present) were quantified. Images were taken from random fields using a HCX PL APO CS 40x/NA1.25 oil objective, and pinhole was opened maximally to allow the entire thickness of the neurite to be imaged. The total number of neurites analyzed ranged from 53 to 346 in each category. Neurite maintenance was represented as the average change in neurite length between day 8 and day 12 of differentiation. At least three independent experiments were performed.

Data analysis

Data from cell viability assays were analyzed by two-way ANOVA. In this case, WT or mutant hSOD1 was used as the between-subjects factor. Comparisons between groups (WT or mutant hSOD1) were made using one-way ANOVA and Tukey's test. All quantified results were expressed as the mean $\pm$ SE. Statistical significance for mitochondria morphology and transport, and neurite length was determined by the Student's two-tailed, unpaired *t*-test, and a *P*-value <0.05 was considered indicative of a significant difference. All statistical *P*-values in this study were determined using ANOVA or *t*-test from experiments repeated a minimum of three times, unless stated otherwise.

ACKNOWLEDGEMENTS

We thank Dr. Carla Koehler for providing the yeast cytochrome b2 construct used in this study, and Dr. Neil R. Cashman for providing the NSC34 cells. We also thank Dr. Roy Smith and Dr. Cristofol Vives-Bauza for critically reading the manuscript.

Conflict of Interest statement. None declared.

FUNDING

This work was supported by National Institute of Health (grants P01-NS011766, NS051419, to G.M.); the Muscular Dystrophy Association (to J.M.); the Robert Packard ALS Research Center 'The New York Community Trust' (to G.M.); the Hiller Foundation (to G.M.); and a Ministerio de Educación y Ciencia postdoctoral fellowship from the Spanish Government (to I.H.).

REFERENCES

1. Bruijn, L.I., Miller, T.M. and Cleveland, D.W. (2004) Unraveling the mechanisms involved in motor neuron degeneration in Als. *Annu. Rev. Neurosci.*, **27**, 723–749.
2. Hervias, I., Beal, M.F. and Manfredi, G. (2006) Mitochondrial dysfunction and amyotrophic lateral sclerosis. *Muscle Nerve*, **33**, 598–608.
3. Magrane, J. and Manfredi, G. (2009) Mitochondrial function, morphology, and axonal transport in amyotrophic lateral sclerosis. *Antioxid. Redox Signal.*, **11**, 1615–1626.
4. Jung, C., Higgins, C.M. and Xu, Z. (2002) A quantitative histochemical assay for activities of mitochondrial electron transport chain complexes in mouse spinal cord sections. *J. Neurosci. Methods*, **114**, 165–172.
5. Mattiazzi, M., D'Aurelio, M., Gajewski, C.D., Martushova, K., Kiaei, M., Beal, M.F. and Manfredi, G. (2002) Mutated human SOD1 causes dysfunction of oxidative phosphorylation in mitochondria of transgenic mice. *J. Biol. Chem.*, **277**, 29626–29633.
6. Kirkinezos, I.G., Bacman, S.R., Hernandez, D., Oca-Cossio, J., Arias, L.J., Perez-Pinzon, M.A., Bradley, W.G. and Moraes, C.T. (2005) Cytochrome c association with the inner mitochondrial membrane is impaired in the CNS of G93A-SOD1 mice. *J. Neurosci.*, **25**, 164–172.
7. Damiano, M., Starkov, A.A., Petri, S., Kipiani, K., Kiaei, M., Mattiazzi, M., Flint Beal, M. and Manfredi, G. (2006) Neural mitochondrial Ca^{2+} capacity impairment precedes the onset of motor symptoms in G93A Cu/Zn-superoxide dismutase mutant mice. *J. Neurochem.*, **96**, 1349–1361.
8. Menzies, F.M., Cookson, M.R., Taylor, R.W., Turnbull, D.M., Chrzanowska-Lightowlers, Z.M., Dong, L., Figlewicz, D.A. and Shaw, P.J. (2002) Mitochondrial dysfunction in a cell culture model of familial amyotrophic lateral sclerosis. *Brain*, **125**, 1522–1533.
9. Kong, J. and Xu, Z. (1998) Massive mitochondrial degeneration in motor neurons triggers the onset of amyotrophic lateral sclerosis in mice expressing a mutant SOD1. *J. Neurosci.*, **18**, 3241–3250.
10. Gould, T.W., Buss, R.R., Vinsant, S., Prevette, D., Sun, W., Knudson, C.M., Milligan, C.E. and Oppenheim, R.W. (2006) Complete dissociation of motor neuron death from motor dysfunction by Bax deletion in a mouse model of ALS. *J. Neurosci.*, **26**, 8774–8786.
11. Sasaki, S. and Iwata, M. (1996) Impairment of fast axonal transport in the proximal axons of anterior horn neurons in amyotrophic lateral sclerosis. *Neurology*, **47**, 535–540.
12. Ligon, L.A., LaMonte, B.H., Wallace, K.E., Weber, N., Kalb, R.G. and Holzbaur, E.L. (2005) Mutant superoxide dismutase disrupts cytoplasmic dynein in motor neurons. *Neuroreport*, **16**, 533–536.
13. Weisiger, R.A. and Fridovich, I. (1973) Superoxide dismutase. Organelle specificity. *J. Biol. Chem.*, **248**, 3582–3592.
14. Sturtz, L.A., Diekert, K., Jensen, L.T., Lill, R. and Culotta, V.C. (2001) A fraction of yeast cu,zn-superoxide dismutase and its metallochaperone, ccs, localize to the intermembrane space of mitochondria. a physiological role for sod1 in guarding against mitochondrial oxidative damage. *J. Biol. Chem.*, **276**, 38084–38089.
15. Okado-Matsumoto, A. and Fridovich, I. (2001) Subcellular distribution of superoxide dismutases (SOD) in rat liver: Cu,Zn-SOD in mitochondria. *J. Biol. Chem.*, **276**, 38388–38393.
16. Jaarsma, D., Rognoni, F., van Duijn, W., Verspaget, H.W., Haasdijk, E.D. and Holstege, J.C. (2001) CuZn superoxide dismutase (SOD1) accumulates in vacuolated mitochondria in transgenic mice expressing amyotrophic lateral sclerosis-linked SOD1 mutations. *Acta Neuropathol. (Berl)*, **102**, 293–305.
17. Higgins, C.M., Jung, C., Ding, H. and Xu, Z. (2002) Mutant Cu, Zn superoxide dismutase that causes motoneuron degeneration is present in mitochondria in the CNS. *J. Neurosci.*, **22**, RC215.

18. Higgins, C.M., Jung, C. and Xu, Z. (2003) ALS-associated mutant SOD1G93A causes mitochondrial vacuolation by expansion of the intermembrane space and by involvement of SOD1 aggregation and peroxisomes. *BMC Neurosci.*, **4**, 16.
19. Vijayvergiya, C., Beal, M.F., Buck, J. and Manfredi, G. (2005) Mutant superoxide dismutase 1 forms aggregates in the brain mitochondrial matrix of amyotrophic lateral sclerosis mice. *J. Neurosci.*, **25**, 2463–2470.
20. Kawamata, H. and Manfredi, G. (2008) Different regulation of wild-type and mutant Cu,Zn superoxide dismutase localization in mammalian mitochondria. *Hum. Mol. Genet.*, **17**, 3303–3317.
21. Vande Velde, C., Miller, T.M., Cashman, N.R. and Cleveland, D.W. (2008) Selective association of misfolded ALS-linked mutant SOD1 with the cytoplasmic face of mitochondria. *Proc. Natl. Acad. Sci. USA*, **105**, 4022–4027.
22. Liu, J., Lillo, C., Jonsson, P.A., Velde, C.V., Ward, C.M., Miller, T.M., Subramaniam, J.R., Rothstein, J.D., Marklund, S., Andersen, P.M. *et al.* (2004) Toxicity of familial ALS-linked SOD1 mutants from selective recruitment to spinal mitochondria. *Neuron*, **43**, 5–17.
23. Son, M., Puttaparthi, K., Kawamata, H., Rajendran, B., Boyer, P.J., Manfredi, G. and Elliott, J.L. (2007) Overexpression of CCS in G93A-SOD1 mice leads to accelerated neurological deficits with severe mitochondrial pathology. *Proc. Natl. Acad. Sci. USA*, **104**, 6072–6077.
24. Ono, H., Gruhler, A., Stuart, R.A., Guiard, B., Schwarz, E. and Neupert, W. (1995) Sorting of cytochrome b2 to the intermembrane space of mitochondria. Kinetic analysis of intermediates demonstrates passage through the matrix. *J. Biol. Chem.*, **270**, 16932–16938.
25. Cashman, N.R., Durham, H.D., Blusztajn, J.K., Oda, K., Tabira, T., Shaw, I.T., Dahrouge, S. and Antel, J.P. (1992) Neuroblastoma x spinal cord (NSC) hybrid cell lines resemble developing motor neurons. *Dev. Dyn.*, **194**, 209–221.
26. Eggett, C.J., Crosier, S., Manning, P., Cookson, M.R., Menzies, F.M., McNeil, C.J. and Shaw, P.J. (2000) Development and characterisation of a glutamate-sensitive motor neurone cell line. *J. Neurochem.*, **74**, 1895–1902.
27. Bruijn, L.I., Becher, M.W., Lee, M.K., Anderson, K.L., Jenkins, N.A., Copeland, N.G., Sisodia, S.S., Rothstein, J.D., Borchelt, D.R., Price, D.L. *et al.* (1997) ALS-linked SOD1 mutant G85R mediates damage to astrocytes and promotes rapidly progressive disease with SOD1-containing inclusions. *Neuron*, **18**, 327–338.
28. Pasinelli, P., Borchelt, D.R., Houseweart, M.K., Cleveland, D.W. and Brown, R.H. Jr (1998) Caspase-1 is activated in neural cells and tissue with amyotrophic lateral sclerosis-associated mutations in copper-zinc superoxide dismutase [published erratum appears in Proc Natl Acad Sci USA 1999 Mar 16;96(6):3330]. *Proc. Natl. Acad. Sci. USA*, **95**, 15763–15768.
29. Barrientos, A. and Moraes, C.T. (1999) Titrating the effects of mitochondrial complex I impairment in the cell physiology. *J. Biol. Chem.*, **274**, 16188–16197.
30. Wong, P.C., Pardo, C.A., Borchelt, D.R., Lee, M.K., Copeland, N.G., Jenkins, N.A., Sisodia, S.S., Cleveland, D.W. and Price, D.L. (1995) An adverse property of a familial ALS-linked SOD1 mutation causes motor neuron disease characterized by vacuolar degeneration of mitochondria. *Neuron*, **14**, 1105–1116.
31. De Vos, K.J., Chapman, A.L., Tennant, M.E., Manser, C., Tudor, E.L., Lau, K.F., Brownlees, J., Ackerley, S., Shaw, P.J., McLoughlin, D.M. *et al.* (2007) Familial amyotrophic lateral sclerosis-linked SOD1 mutants perturb fast axonal transport to reduce axonal mitochondria content. *Hum. Mol. Genet.*, **16**, 2720–2728.
32. Raimondi, A., Mangolini, A., Rizzardini, M., Tartari, S., Massari, S., Bendotti, C., Francolini, M., Borgese, N., Cantoni, L. and Pietrini, G. (2006) Cell culture models to investigate the selective vulnerability of motoneuronal mitochondria to familial ALS-linked G93ASOD1. *Eur. J. Neurosci.*, **24**, 387–399.
33. Xu, Z., Jung, C., Higgins, C., Levine, J. and Kong, J. (2004) Mitochondrial degeneration in amyotrophic lateral sclerosis. *J. Bioenerg. Biomembr.*, **36**, 395–399.
34. Pasinelli, P. and Brown, R.H. (2006) Molecular biology of amyotrophic lateral sclerosis: insights from genetics. *Nat. Rev. Neurosci.*, **7**, 710–723.
35. Rizzardini, M., Mangolini, A., Lupi, M., Ubezio, P., Bendotti, C. and Cantoni, L. (2005) Low levels of ALS-linked Cu/Zn superoxide dismutase increase the production of reactive oxygen species and cause mitochondrial damage and death in motor neuron-like cells. *J. Neurol. Sci.*, **232**, 95–103.
36. Ferri, A., Cozzolino, M., Crosio, C., Nencini, M., Casciati, A., Gralla, E.B., Rotilio, G., Valentine, J.S. and Carri, M.T. (2006) Familial ALS-superoxide dismutases associate with mitochondria and shift their redox potentials. *Proc. Natl. Acad. Sci. USA*, **103**, 13860–13865.
37. Cozzolino, M., Pesaresi, M.G., Amori, I., Crosio, C., Ferri, A., Nencini, M. and Carri, M.T. (2009) Oligomerization of mutant SOD1 in mitochondria of motoneuronal cells drives mitochondrial damage and cell toxicity. *Antioxid. Redox Signal.*, **11**, 1547–1558.
38. Estevez, A.G., Crow, J.P., Sampson, J.B., Reiter, C., Zhuang, Y., Richardson, G.J., Tarpey, M.M., Barbeito, L. and Beckman, J.S. (1999) Induction of nitric oxide-dependent apoptosis in motor neurons by zinc-deficient superoxide dismutase. *Science*, **286**, 2498–2500.
39. Martin, L.J., Liu, Z., Chen, K., Price, A.C., Pan, Y., Swaby, J.A. and Golden, W.C. (2007) Motor neuron degeneration in amyotrophic lateral sclerosis mutant superoxide dismutase-1 transgenic mice: mechanisms of mitochondriopathy and cell death. *J. Comp. Neurol.*, **500**, 20–46.
40. Deng, H.X., Shi, Y., Furukawa, Y., Zhai, H., Fu, R., Liu, E., Gorrie, G.H., Khan, M.S., Hung, W.Y., Bigio, E.H. *et al.* (2006) Conversion to the amyotrophic lateral sclerosis phenotype is associated with intermolecular linked insoluble aggregates of SOD1 in mitochondria. *Proc. Natl. Acad. Sci. USA*, **103**, 7142–7147.
41. Kawamata, H., Magrane, J., Kunst, C., King, M.P. and Manfredi, G. (2008) Lysyl-tRNA synthetase is a target for mutant SOD1 toxicity in mitochondria. *J. Biol. Chem.*, **283**, 28321–28328.
42. Pasinelli, P., Belford, M.E., Lennon, N., Bacskai, B.J., Hyman, B.T., Trotti, D. and Brown, R.H. Jr (2004) Amyotrophic lateral sclerosis-associated SOD1 mutant proteins bind and aggregate with Bcl-2 in spinal cord mitochondria. *Neuron*, **43**, 19–30.
43. Zhang, F., Strom, A.L., Fukada, K., Lee, S., Hayward, L.J. and Zhu, H. (2007) Interaction between familial ALS-linked SOD1 mutants and the dynein complex: Implications of retrograde axonal transport in ALS. *J. Biol. Chem.*, **282**, 16691–16699.
44. Fischer, L.R., Culver, D.G., Tennant, P., Davis, A.A., Wang, M., Castellano-Sanchez, A., Khan, J., Polak, M.A. and Glass, J.D. (2004) Amyotrophic lateral sclerosis is a distal axonopathy: evidence in mice and man. *Exp. Neurol.*, **185**, 232–240.
45. Chiesa, A., Rapizzi, E., Tosello, V., Pinton, P., de Virgilio, M., Fogarty, K.E. and Rizzuto, R. (2001) Recombinant aequorin and green fluorescent protein as valuable tools in the study of cell signalling. *Biochem. J.*, **355**, 1–12.
46. Manfredi, G., Yang, L., Gajewski, C.D. and Mattiazzi, M. (2002) Measurements of ATP in mammalian cells. *Methods*, **26**, 317–326.